Characterizing the 2010 Russian heatwave-Pakistan floo extreme over the last millennium using the Great Eurasiar

Benjamin I Cook[1,2] and Edward R Cook[2] and Kevin J Anchukaitis[2,3,4] and Deepti Singh[5]

[1]*NASA Goddard Institute for Space Studies, New York, New York, USA*

[2]*Lamont-Doherty Earth Observatory, Palisades, New York, USA*

[3]*Laboratory for Tree Ring Research, University of Arizona, Tucson, Arizona, USA*

[4]*School of Geography, Development and Environment, University of Arizona, Tucson, Arizona, USA*

[5]*School of the Environment, Washington State University Vancouver, Vancouver, Washington, USA*

Corresponding author: Benjamin I Cook, benjamin.i.cook@nasa.gov

Early Online Release: This preliminary version has been accepted for publication in *Journal of Climate*, may be fully cited, and has been assigned DOI 10.1175/JCLI-D-23-0773.1. The final typeset copyedited article will replace the EOR at the above DOI when it is published.

ABSTRACT: During summer 2010, exceptional heat and drought in western Russia (WRU) occurred simultaneously with heavy rainfall and flooding in northern Pakistan (NPK). Here, we use the Great Eurasian Drought Atlas (GEDA), a new 1,021 year tree-ring reconstruction of summer soil moisture, to investigate the variability and dynamics of this exceptional spatially concurrent climate extreme over the last millennium. Summer 2010 in the GEDA was the second driest year over WRU and the largest wet–dry contrast between NPK and WRU; it was also the second warmest year over WRU in an independent 1,015 year temperature reconstruction. Soil moisture variability is only weakly correlated between the two regions and 2010 event analogues are rare, occurring in 31 (3.0%) or 52 (5.1%) years in the GEDA, depending on the definition used. Post-1900 is significantly drier in WRU and wetter in NPK compared to previous centuries, increasing the likelihood of concurrent wet NPK–dry WRU extremes, with over 20% of the events in the record occurring in this interval. The dynamics of wet NPK–dry WRU events like 2010 are well captured by two principal components in the GEDA, modes correlated with ridging over northern Europe and western Russia and a pan-hemispheric extratropical wave train pattern similar to that observed in 2010. Our results highlight how high resolution paleoclimate reconstructions can be used to capture some of the most extreme events in the climate system, investigate their physical drivers, and allow us to assess their behavior across longer timescales than available from shorter instrumental records.

Accepted for publication in *Journal of Climate*. DOI 10.1175/JCLI-D-23-0773.1.

1. Introduction

In the summer of 2010, Eurasia experienced a spatially concurrent extreme climate event, characterized by severe drought and heat over western Russia and heavy precipitation and flooding over northern Pakistan (Dole et al. 2011; Lau and Kim 2012; Webster et al. 2011). Europe and western Russia experienced one of the hottest summers of the last 500 years (Barriopedro et al. 2011), with pervasive impacts across the region including over 11,000 excess deaths from heat and wildfire smoke (Shaposhnikov et al. 2014) and a 34% reduction in wheat production compared to the previous two years (Hunt et al. 2021). The Pakistan floods affected over 20 million people, resulting in over 1,000 human deaths, the loss of 20,000 cattle, and estimated damages of $US 40 billion (Houze et al. 2011; Lau and Kim 2012; Webster et al. 2011).

The main driver of this spatially concurrent extreme was a circumglobal Rossby wave train in the atmosphere. This gave rise to a persistent ridge over western Russia, amplifying heat and drought through anomalous subsidence and suppression of precipitation, and a trough over northern Pakistan that caused a series of extreme rainfall events (Di Capua et al. 2021; Lau and Kim 2012). These waves, and the related dynamics, are one of the main drivers of summer season climate extremes over extratropical Eurasia (Schubert et al. 2014). For 2010, the occurrence of this wave train was favored by both the state of the tropical oceans, including a La Niña in the tropical Pacific and a negative Indian Ocean Dipole (IOD), and high latitude warming (Di Capua et al. 2021). Dry soil moisture conditions in western Russia likely further amplified extreme heat in this region (Christian et al. 2020; Hauser et al. 2016; Lau and Kim 2012; Miralles et al. 2014) and may have enhanced heavy rainfall in northern Pakistan by reinforcing the wave response (Di Capua et al. 2021). Indian Ocean sea surface temperatures also likely increased advection of moisture that fed into the heavy rainfall in northern Pakistan (Priya et al. 2015).

The 2010 concurrent extreme was an exceptional event, but understanding how it compares to long-term variability in the climate system is limited by the relatively short length of the observational record and the difficulty many models have in simulating extreme events and their related dynamics (Angélil et al. 2016; White et al. 2022). Here, we demonstrate that events analogous to 2010 can be found in a new spatial, tree-ring based reconstruction of summer season (June-July-August; JJA) soil moisture, the Great Eurasian Drought Atlas (GEDA), allowing us analyze 2010 in the context of the last 1,021 years. We focus on the following research questions: (1) How

Accepted for publication in *Journal of Climate*. DOI 10.1175/JCLI-D-23-0773.1.

extreme were the soil moisture anomalies during the 2010 event compared to the last millennium?; (2) How often have similar events occurred in the past, and is their risk increasing?; and (3) What modes of variability in the GEDA are most closely connected to 2010-type concurrent events, and how are they related to atmospheric circulation and sea surface temperatures (SSTs)?

2. Materials and Methods

a. Great Eurasian Drought Atlas (GEDA)

The GEDA is a new, tree-ring based reconstruction of summer season (JJA) self-calibrating Palmer Drought Severity Index (PDSI) (Wells et al. 2004). PDSI is a normalized soil moisture index (Palmer 1965), accounting for changes in both supply (precipitation) and demand (evaporative losses), with intrinsic memory and persistence from month-to-month. The reconstruction itself targets the latest version of the PDSI dataset produced by the Climate Research Unit (CRU) of the University of East Anglia (Barichivich et al. 2022; van der Schrier et al. 2013), based on version 4.06 of the CRU TS monthly high-resolution gridded multivariate climate dataset (Harris et al. 2020). The GEDA builds, expands, and improves upon previous spatial reconstructions of PDSI, including the Old World Drought Atlas (Cook et al. 2015), the Monsoon Asia Drought Atlas (Cook et al. 2010), and the European Russia Drought Atlas (Cook et al. 2020b).

The GEDA was produced on a 37,774 point 0.5^{o}x0.5^{o} grid of PDSI data covering the entire Eurasian region and a substantial portion of sub-Saharan Africa from a network of 1,869 tree-ring chronologies and one annually layered speleothem record from Oman (Supplementary Figure 1). It is based on a variant of Ensemble Point-by-Point Regression (EPPR) that optimizes each grid point reconstruction based on the 'out-of-sample' validation period R2 (VRSQ). This is performed over a range of search radii and power weightings applied to the correlations between the tree-ring data and each grid point PDSI record over the 1951-1990 calibration period with the 1920–1950 period data withheld for validation testing. There is no a priori 'best' search radius or power weighting for all grid points because of the highly variable spatial density of the tree-ring network shown in Supplementary Figure 1. The GEDA's substantial mix of tree species used for reconstruction across the network further complicates the reconstruction process.

EPPR applied this way produces a total of 48 'candidate' reconstruction models from which the 'best' model in terms of validation period VRSQ is then selected. This EPPR approach is

Accepted for publication in *Journal of Climate*. DOI 10.1175/JCLI-D-23-0773.1.

summarized in the flowchart schematic in Supplementary Figure 2, and the reader is referred to Smerdon et al. (2023) for more details. Applied this way, EPPR is a form of 'supervised machine learning' (Bortnik and Camporeale 2021) that seeks the optimal pointwise models for reconstructing PDSI across the GEDA target field. As the number of available chronologies declines further in the past, the reconstruction model is systematically recalibrated beginning on or before 1800, 1700, 1600, 1500, 1400, 1300, 1200, 1100, or 1000 CE, for nine cutoffs in total, using only chronologies available at the cutoff year. Maps showing the stability of VRSQ across the GEDA domain are shown for the 1800, 1600, and 1400 cutoffs in Supplementary Figure 3. The overall stability and validation statistics of the reconstruction are excellent, especially over western Russia and northern Pakistan where this study is focused. This process resulted in a 9-member ensemble of 'best' GEDA reconstructions which were then averaged to produce the final GEDA used in this study. In the process, each grid point average reconstruction was recalibrated and revalidated, thus producing the final GEDA calibration and validation maps shown in Supplementary Figure 4.

The full GEDA dataset covers the time period of 1000–2020 CE, with tree-ring reconstructed values spanning 1000–1989 CE and instrumental observations from 1990–2020 CE. Based on the scope of our analyses, which is focused on the 2010 concurrent extreme event over Eurasia, we do not consider the GEDA domain for Sub-Saharan Africa and south of the equator. We also restandardized PDSI at every grid cell to a mean of zero and unit standard deviation (z-scores) using the entire period as the baseline (1000–2020 CE) so that all soil moisture values are expressed in units of standard deviation (σ).

b. NTREND Temperature Reconstruction

We used the Northern Hemisphere Tree-Ring Network Development (NTREND) spatial reconstruction of extra-tropical (40–90^{o}N) boreal summer (May-June-July-August; MJJA) mean temperature from Anchukaitis et al. (2017). The reconstruction uses a simplified non-ensemble version of the PPR technique described above applied to a network of 54 temperature-sensitive tree-ring chronologies and individual tree-ring temperature reconstructions to estimate summer temperatures on the regular 5 degree grid from the interpolated hybrid (surface and satellite information) version of HadCRUT4 from Cowtan and Way (2014) and Morice et al. (2012). NTREND covers the period from 750 to 2014 CE, with tree-ring reconstructed values spanning 750–1988 CE and

Accepted for publication in *Journal of Climate*. DOI 10.1175/JCLI-D-23-0773.1.

instrumental observations from 1989–2014 CE. Specifics on data, methods, and results are available from Wilson et al. (2016) and Anchukaitis et al. (2017). For our analysis here, we extract and average the NTREND temperature values from 48–64°N and 42–66°E to represent western Russia for the maximum years overlapping with the GEDA (1000–2014 CE). Although a rescaling step in NTREND accounts for the statistical effect of variances changes due to declining sample size at each individual grid point in the reconstruction, we apply a bias correction using quantile regression (Robeson et al. 2020) to the regional western Russian average to ensure the regional average is comparable through time. NTREND does not include the Pakistan domain we used in the GEDA, due to a paucity of temperature-sensitive trees near this region (Anchukaitis et al. 2017; Esper et al. 2018; Wilson et al. 2016).

While it is fairly straightforward to trace the influence of the NTREND predictor data to the reconstructed temperatures in the study region, it is more difficult to do this for GEDA because of the components of the ensemble approach used. However, there are several factors that likely mean there is little shared information between the two reconstructions. First and foremost, the NTREND predictors are high latitude positive temperature responders positively correlated with their local summer temperature (see Wilson et al. (2016) and Anchukaitis et al. (2017)). They are also mostly density-based proxies or proxy reconstructions, which are known to reflect summer and late summer temperatures. Second, the weak relationship at the interannual scale shown later in Figures 2 and 3 between NTREND temperature and GEDA PDSI in western Russia suggests there could not be much sharing of information. This overall weak coupling would be unlikely if there was sharing of information between the two paleoclimate field reconstructions. Third, the weak relationship shown in Figure 3 is similar to that seen in studies where we have been able to use individual chronologies to reconstruct different targets (e.g. high altitude density and low elevation ring width for temperature and PDSI in Mongolia from Pederson et al. (2014)). Finally, the year of interest (2010) is outside the period covered by the tree-ring proxies in both GEDA and NTREND and so comes from instrumental data. Thus the primary comparison of interest for the temperature data is (1) in comparison to temperatures in the past millennium and (2) with years of extreme drought in the GEDA record.

Accepted for publication in *Journal of Climate*. DOI 10.1175/JCLI-D-23-0773.1.

c. Observational Data

We used the latest versions (4.07 for temperature and precipitation, 4.06 for PDSI) of the CRU climate grids (Harris et al. 2020) to demonstrate that the 2010 concurrent extreme can be represented in JJA seasonal average anomalies of maximum temperature, precipitation, and soil moisture (PDSI). PDSI is not yet available from the most recent version of the climate grids, which is why the prior version is used. We also used 300 hPa geopotential heights and meridional winds from version 3 of the Twentieth Century Reanalysis (Slivinski et al. 2021) and SSTs from HadiSST (Rayner et al. 2003) to analyze the dynamics of the 2010 event and compare against variability in the GEDA.

3. Results

a. Observed Climate During the 2010 Concurrent Event

The 2010 concurrent climate extreme over Eurasia is well resolved in the JJA seasonal average observed anomalies of maximum temperature, precipitation, and soil moisture (Figure 1). Maximum temperature and precipitation anomalies are all relative to a 1901–2022 baseline, spanning the entirety of this observational record. The PDSI are from the observational portion of the GEDA, where each grid cell is restandardized to a mean of zero and unit standard deviation using the entire GEDA record (1000–2020 CE). Dashed boxes outline the main centers of action for the 2010 event which we focus our analyses around: western Russia (WRU: 42°E–66°E; 48°N–64°N) and Central Asia and northern Pakistan (NPK: 67°E–80°E; 32°N–46°N). We chose these regions because (1) they are areas where some of the largest impacts of the 2010 event emerged, (2) previous work has established the presence of dynamical connections between these regions, and (3) these areas include some of the most intense soil moisture anomalies that occurred during this event.

Higher than normal maximum temperature anomalies extend across Europe and the Middle East, peaking in intensity within the WRU region, while temperatures are cooler than normal over parts of high latitude Asia and the NPK region. Precipitation anomalies show strong deficits in a broad area around the Caspian Sea, extending northward across WRU, corresponding closely with the areas that have some of the highest maximum temperature anomalies. By contrast, extremely large precipitation surpluses occur across most of Pakistan, including up into the NPK region. The integrative soil moisture responses closely reflect the temperature and precipitation anomalies,

Accepted for publication in *Journal of Climate*. DOI 10.1175/JCLI-D-23-0773.1.

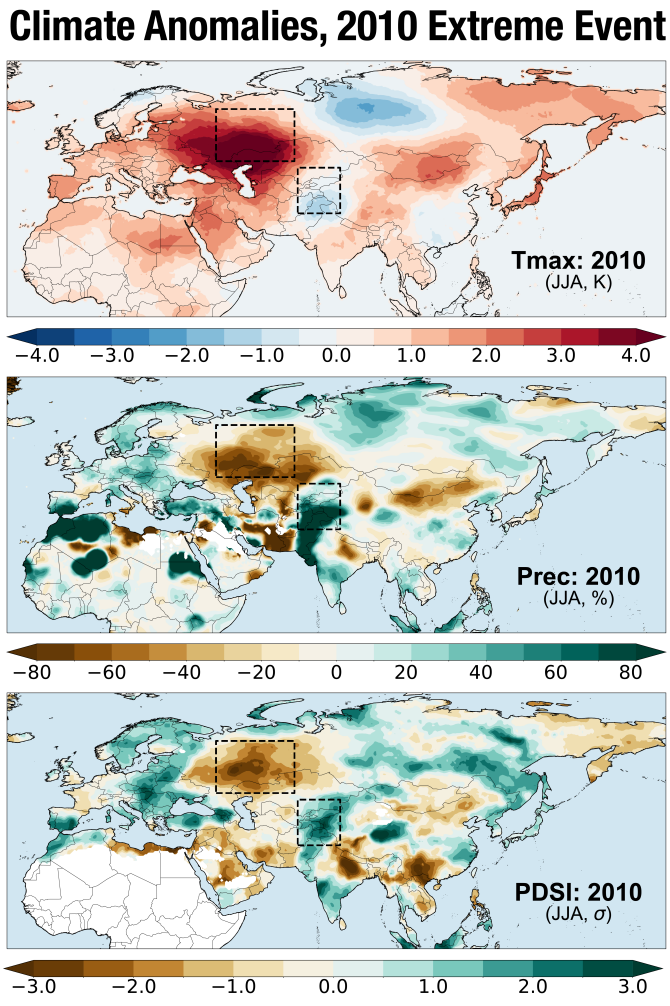

FIG. 1. Summer (JJA) 2010 seasonal average anomalies of maximum temperature (K), precipitation (%), and soil moisture (PDSI, σ) from the CRU climate grids and GEDA. Dashed boxes indicate regions of focus for our analyses: western Russia (WRU: 42°E–66°E; 48°N–64°N) and Central Asia and northern Pakistan (NPK: 67°E–80°E; 32°N–46°N). While the extreme heat in WRU and rainfall in NPK were subseasonal events, this analysis demonstrates that they are detectable at the seasonal scale. This includes the seasonal soil moisture conditions, reflected by the PDSI, which show severe drought over WRU and high soil moisture over NPK.

with intense drought over WRU and substantially wetter than normal conditions over NPK, though there is not complete overlap across the different fields. This reflects, to some extent, the nature of the soil moisture calculation in PDSI, which has a long intrinsic memory sensitive to moisture balance changes (precipitation and evapotranspiration) in prior months and seasons. Combined with the fact that the extreme seasonal rainfall anomaly in NPK is driven primarily by three multi-

Accepted for publication in *Journal of Climate*. DOI 10.1175/JCLI-D-23-0773.1.

day periods of intense precipitation in July (Lau and Kim 2012), some inconsistency between the precipitation and PDSI fields will be expected. Despite these different temporal scales, however, these results demonstrate that the sub-seasonal extremes driving the 2010 concurrent extreme are captured by the seasonal soil moisture anomalies targeted in the GEDA reconstruction.

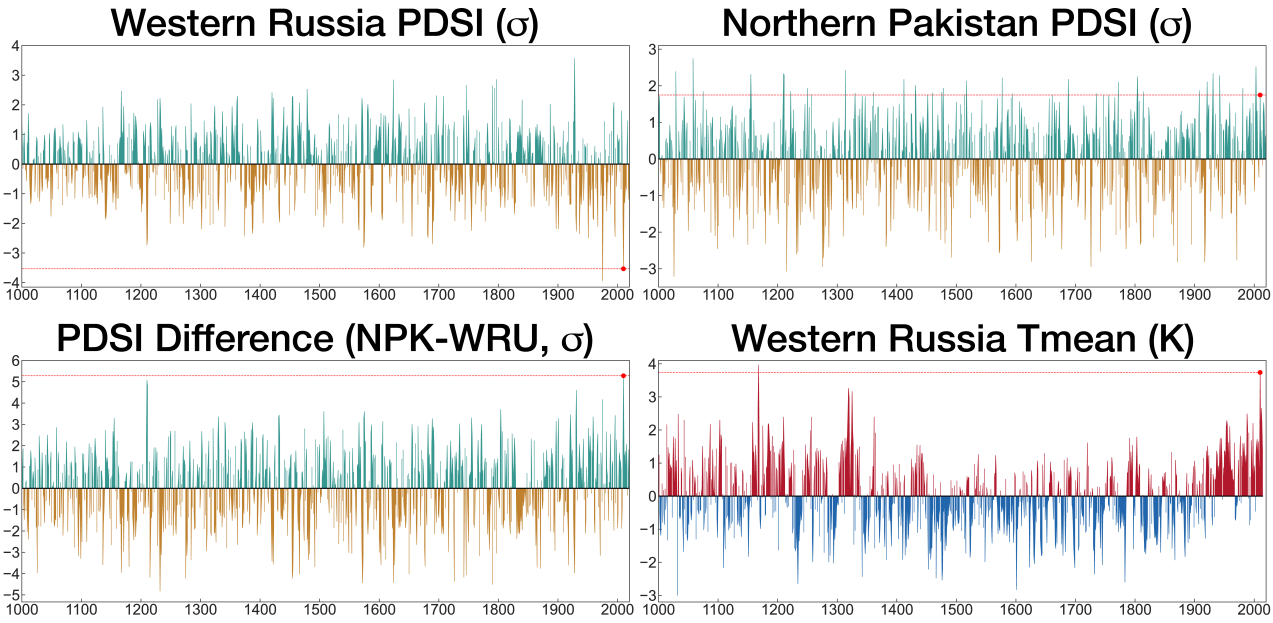

FIG. 2. Time series of soil moisture (PDSI; σ) in the GEDA averaged over WRU and NPK, the difference between these two series (NPK minus WRU), and NTREND reconstructed mean temperature (K). WRU and NPK soil moisture series were restandardized to a mean of zero and unit standard deviation over the entire record (1000–2020 CE) after area-weighted spatial averaging. NTREND temperature anomalies (K) are centered around a 1000–2014 CE baseline, the maximum length of this reconstruction.

b. WRU and NPK Soil Moisture Variability in the GEDA

Soil moisture and mean temperature anomalies during 2010 stand out as extreme relative to variability over the last millennium (Figure 2). WRU soil moisture in 2010 was the second driest in the entire 1,021 year long record ($-3.53\ \sigma$), exceeded only by another major Russian drought in 1975 that contributed to large-scale famine across the region (Wright 1975). The extreme high soil moisture in NPK was more muted ($+1.75\ \sigma$), but still ranked above the 96$^{\text{th}}$ percentile for all years in the record. Consequently, these two regions experienced the single largest wet-dry contrast in the entire record in 2010 (NPK minus WRU; $+5.28\ \sigma$). Summer 2010 in WRU was also the second

Accepted for publication in *Journal of Climate*. DOI 10.1175/JCLI-D-23-0773.1.

warmest year in the record (+3.74 K) in the NTREND temperature reconstruction, slightly cooler than 1168 CE, the single warmest year in WRU and in the entire NTREND reconstruction in the pre-industrial period (Anchukaitis et al. 2017; Wilson et al. 2016).

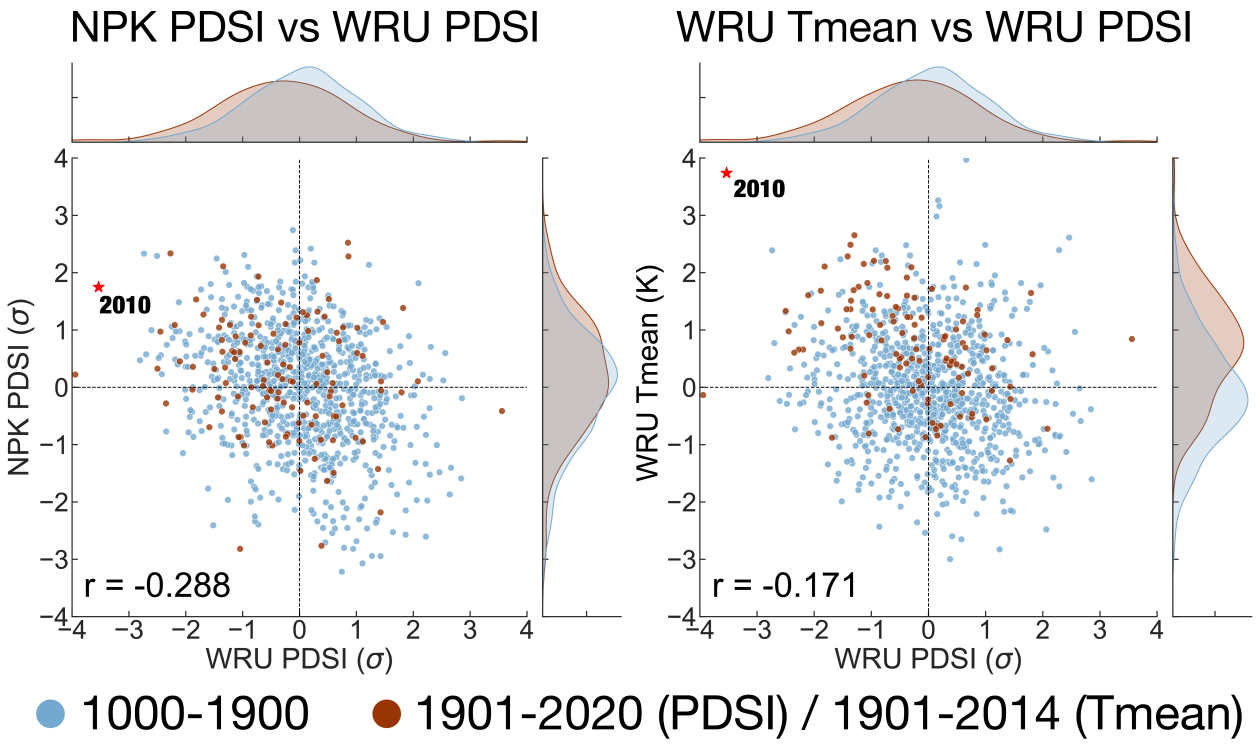

FIG. 3. Joint scatter and kernel density plots comparing soil moisture (PDSI) and mean temperature (Tmean) variability across the WRU and NPK regions: WRU PDSI vs NPK PDSI (left panel) and WRU Tmean vs WRU PDSI (middle panel). Density plots compare distributions of these variables between the the pre- (1000-1900 CE, blue) and post-1900 (1901-2020 for PDSI, 1901-2014 for Tmean; orange) periods. Inset text are Pearson's correlation between the plotted quantities using all available data. The 2010 event is highlighted in the red star.

Soil moisture variability between the two regions is only weakly negatively correlated over the full period of record (1000–2020 CE; Pearson's $r = -0.288$) and the post-1900 interval (1901–2020 CE; Pearson's $r = -0.191$) (Figure 3, left scatter plot), suggesting some tendency towards antiphased anomalies in the regions but an overall weak relationship. The correlation between WRU Tmean and PDSI is also relatively weak (1000–2014 CE; Pearson's $r = -0.171$) (Figure 3, right scatter plot), which appears counter to the evidence that dry soils during 2010 amplified the heat in the region (Christian et al. 2020; Hauser et al. 2016; Lau and Kim 2012; Miralles et al. 2014). More

Accepted for publication in *Journal of Climate*. DOI 10.1175/JCLI-D-23-0773.1.

likely, this low correlation could arise for several reasons: the slight seasonal mismatch between NTREND (MJJA) and PDSI (JJA); the limitations of using seasonal average metrics to study subseasonal events; the relatively high monthly persistence in the PDSI soil moisture calculation, which makes this variable more sensitive to precipitation and evaporative demand from antecedent seasons; or the separate tree-ring networks used in NTREND and GEDA, which differ in terms of their spatial distribution and climate sensitivities.

The distribution of soil moisture in both regions, and mean temperature in WRU, has shifted significantly in the post-1900 period to favor the occurrence of wet NPK–dry WRU concurrent events (Figure 3, density plots). Two-sided Wilcoxon Rank Sum and Kolmogorov-Smirnov tests indicate that, compared to 1000–1900 CE, the post-1900 period (1901–2020 CE for soil moisture; 1901–2014 CE for WRU mean temperature) is significantly drier in WRU ($p \leq 0.01$), wetter in NPK ($p \leq 0.05$), and warmer in WRU ($p \leq 0.01$). To investigate if this is influenced by the transition from tree-ring reconstructed to instrumental PDSI in 1990, we repeated the Wilcoxon Rank Sum and Kolmogorov-Smirnov tests restricting the post-1900 soil moisture data to the tree-ring reconstructed interval (1901–1989 CE). For WRU, we still find significant drying using both statistical tests ($p \leq 0.01$), but differences in soil moisture over NPK compared to 1000–1900 CE are insignificant.

Within the GEDA, soil moisture in WRU fell below -1σ in 160 years, while in NPK, soil moisture exceeded $+1\sigma$ in 146 years (Figure 4, top row). Despite the relatively weak correlation in soil moisture variability across the two regions (Figure 3), large anomalies outside WRU and NPK in these single region composites are apparent, suggesting the importance of larger scale forcing and teleconnections for these events. Droughts in WRU are associated with wetter than average conditions in a band spanning across Europe, Anatolia, and Southwest Asia. Wet extremes in NPK coincide with drought conditions in WRU and northern peninsular India and wetter than average conditions in Bangladesh and eastern India.

These teleconnections are even clearer when compositing on concurrent wet NPK–dry WRU events, which we define in two ways (Figure 4, bottom row). First, we define these events as years when PDSI in NPK is $\geq +1\ \sigma$ and PDSI in WRU is $\leq -1\ \sigma$, which yields 31 events. Alternatively, we identify these concurrent extremes as occurring when the magnitude of the difference time series (NPK minus WRU) falls at or above the 95$^{\text{th}}$ percentile for all years, which finds 52 events.

Accepted for publication in *Journal of Climate*. DOI 10.1175/JCLI-D-23-0773.1.

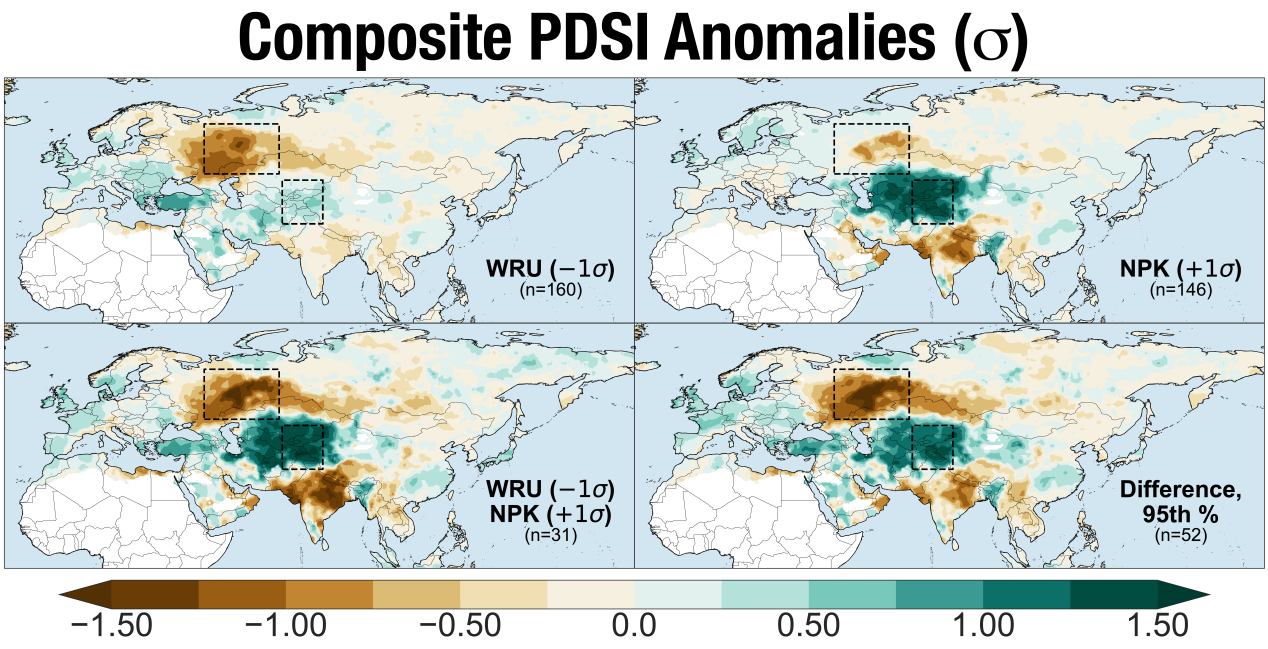

FIG. 4. Composite average soil moisture anomalies (σ) from the GEDA (1000–2020 CE) for single region WRU droughts ($\leq -1\sigma$) and NPK pluvials ($\geq +1\sigma$) (top row) and for two definitions of wet NPK–dry WRU concurrent extremes (bottom row).

Both definitions yield nearly identical intensities and spatial patterns of the soil moisture anomalies within and outside the core NPK and WRU regions.

To assess the degree to which we may expect wet NPK–dry WRU events to happen through random chance alone, we generated a 10,000-member ensemble of simulated soil moisture for WRU and NPK by phase-scrambling each time series in the frequency domain and then transforming back into the time domain. Each synthetic time series will therefore have its own unique temporal evolution while retaining the same frequency characteristics as the original time series from the GEDA. For each iteration, we determined the number of concurrent wet NPK–dry WRU events using both methods described above, and then calculated the 95$^{\text{th}}$ percentile across the ensemble to use as our significance threshold. For the $+/-1\sigma$ wet NPK–dry WRU definition, the 95$^{\text{th}}$ percentile is 33 events and for the difference time series definition it is 45 events. These results suggest the occurrence of wet NPK–dry WRU events does happen more often than would be predicted from random chance alone, at least based on the difference time series definition.

On a percentage basis, concurrent wet NPK–dry WRU extremes occur in 3.0% or 5.1% of all

Accepted for publication in *Journal of Climate*. DOI 10.1175/JCLI-D-23-0773.1.

years (1000–2020 CE), based on the $+/-1\sigma$ and 95th percentile definitions, respectively. However, there is a much higher frequency of these events in the post-1900 period, consistent with the overall shifts in soil moisture in these regions discussed previously (Figure 3). For the $+/-1\sigma$ definition, 9 of the 31 events occur after 1900 (1901, 1921, 1930, 1931, 1943, 1954, 1959, 1988, and 2010). This represents an increase in frequency from 2.4% (22 of 901 years) during 1000–1900 CE to 7.5% (9 of 120 years) in the post-1900 interval, a tripling in frequency. Using our alternative 95th percentile definition, 12 of the 52 events occur post-1900 (1901, 1921, 1930, 1931, 1951, 1959, 1967, 1975, 1981, 1988, 1996, and 2010), representing an increase from 4.4% to 10% of all years in the two periods, a doubling in frequency. While the reconstruction takes advantage of the increased availability of tree-ring chronologies in recent centuries, this is unlikely to be driving the observed increase in event occurrence post-1900. First, all chronologies begin before 1800 CE, and the majority also extend back before 1700 CE. Despite the same or similarly high numbers of chronologies used during these other centuries, event occurrence is much lower compared to post-1900: 3 in the 1700s and 4 in the 1800s. Additionally, the second highest concentration of concurrent events occurs early in the record during the 1300s (9 events). Second, validation statistics in the GEDA reconstruction are generally consistent even as tree-ring availability declines back in time, especially in the main regions of our analysis (Supplementary Figure 3), suggesting an overall stable reconstruction.

c. Dynamics of Single Region Extreme Events

Composite average anomalies of 300 hPa geopotential heights (m), 300 hPa meridional winds (m/s), and SSTs (K) for all -1σ WRU (n=22) and $+1\sigma$ NPK (n=17) soil moisture events during the post-1900 period (1901–2015) are shown in Figure 5. The -1σ WRU events are associated with strong ridging centered over northern Europe and western Russia and amplified meridional wind anomalies from the North Atlantic to South Asia. Local geopotential height anomalies are relatively weaker for the $+1\sigma$ NPK events, and part of a wave-like pattern across Eurasia. These events also appear to be associated with a strong circumglobal wave train based on meridional wind fields that shows some similarity to a Rossby wavenumber 5 (e.g., Luo et al. 2022), a moderate warm anomaly in tropical Pacific SSTs, and a strong dipole in Northeast Pacific SSTs. These composite patterns show a strong resemblance to the first two rotated empirical orthogonal functions (REOFs)

Accepted for publication in *Journal of Climate*. DOI 10.1175/JCLI-D-23-0773.1.

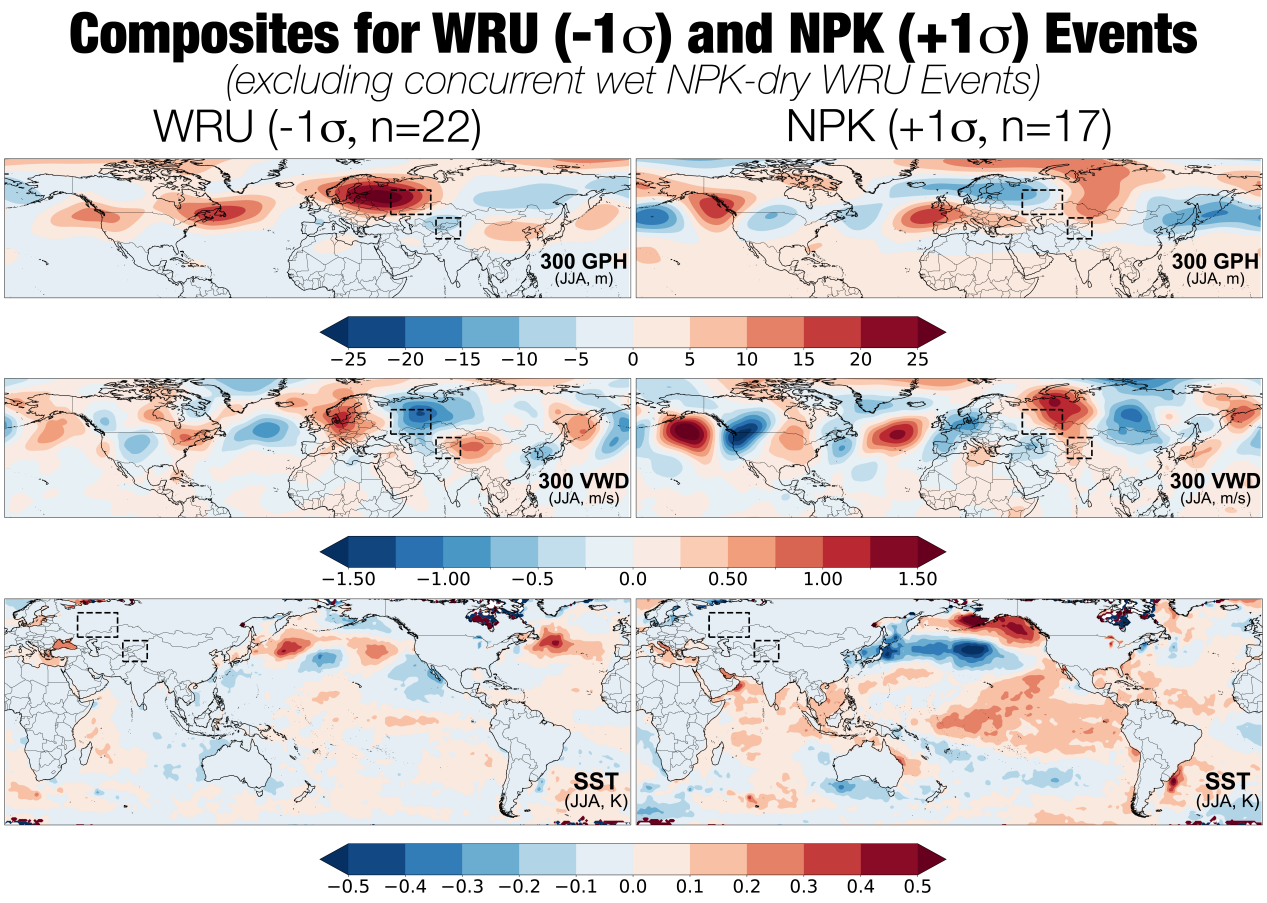

FIG. 5. Composite average (1901–2015) JJA circulation (300 hPa geopotential heights, m; meriodional winds; m/s) and sea surface temperature anomalies (K) for all -1σ WRU (n=22) and $+1\sigma$ NPK (n=17) soil moisture events, excluding years with concurrent wet NPK-dry WRU extremes.

of summer season 250 hPa meridional wind anomalies found previously by Schubert et al. (2011). The loadings for their REOF #1 are also highly localized over Eurasia and this mode is strongly associated with heat and droughts over the area including our WRU region. By contrast, their REOF #2 shows a pan-hemispheric wave train similar to the meridional wind composite for our $+1\sigma$ NPK events.

To further explore the dynamics of these events in the GEDA, we conducted our own REOF analysis on the standardized data matrix of the GEDA PDSI (1000–2020 CE). The leading 7 modes account for 44.9% of the total variance in the GEDA, after which there is a rapid decline in variance explained by any additional mode. We applied varimax rotation to these 7 modes and identified two (#1 and #5) with significant correlations to drought variability in the WRU and NPK

Accepted for publication in *Journal of Climate*. DOI 10.1175/JCLI-D-23-0773.1.

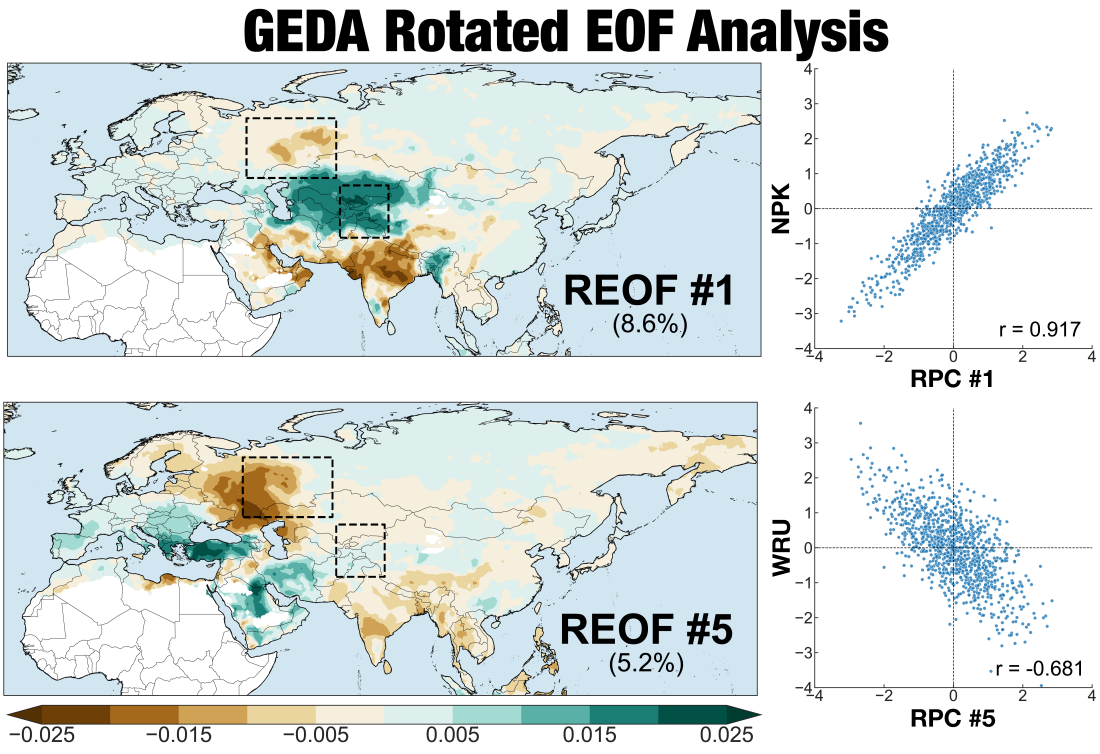

FIG. 6. REOFs (#1 and #5) and associated RPCs (standardized to zero mean and unit standard deviation) from the REOF analysis of the GEDA. Inset percentages on the REOF plots indicate the percent variance associated with these two individual modes. Scatter plots show comparisons and Pearson's r correlations (1000–2020 CE) between the RPCs and PDSI in the regions they load most strongly into: RPC #1 with NPK and RPC #5 with WRU.

regions (Figure 6). REOF #1 has a strong center of action east of the Caspian Sea, including the NPK region, with large magnitude opposite sign loadings across western and central India to the south and more moderate opposite sign loadings in the WRU region. The corresponding rotated principal component (RPC) is strongly positively correlated with NPK PDSI (Pearson's $r = +0.917$) and weakly negatively correlated with WRU PDSI ($r = -0.254$, not shown). REOF #5 has positive loadings across southern and western Europe and Anatolia and negative loadings in the eastern part of WRU. RPC #5 is much more strongly correlated with WRU PDSI compared to RPC #1 (Pearson's $r = -0.681$) and is effectively uncorrelated with NPK PDSI (Pearson's $r = +0.026$).

Correlations between RPCs #1 and #5 and the circulation and SST fields reveal that the dynamics underlying hydroclimate extremes in WRU and NPK are well captured by these modes of variability (Figure 7). Correlations with RPC #1, the mode strongly positively correlated with NPK soil

Accepted for publication in *Journal of Climate*. DOI 10.1175/JCLI-D-23-0773.1.

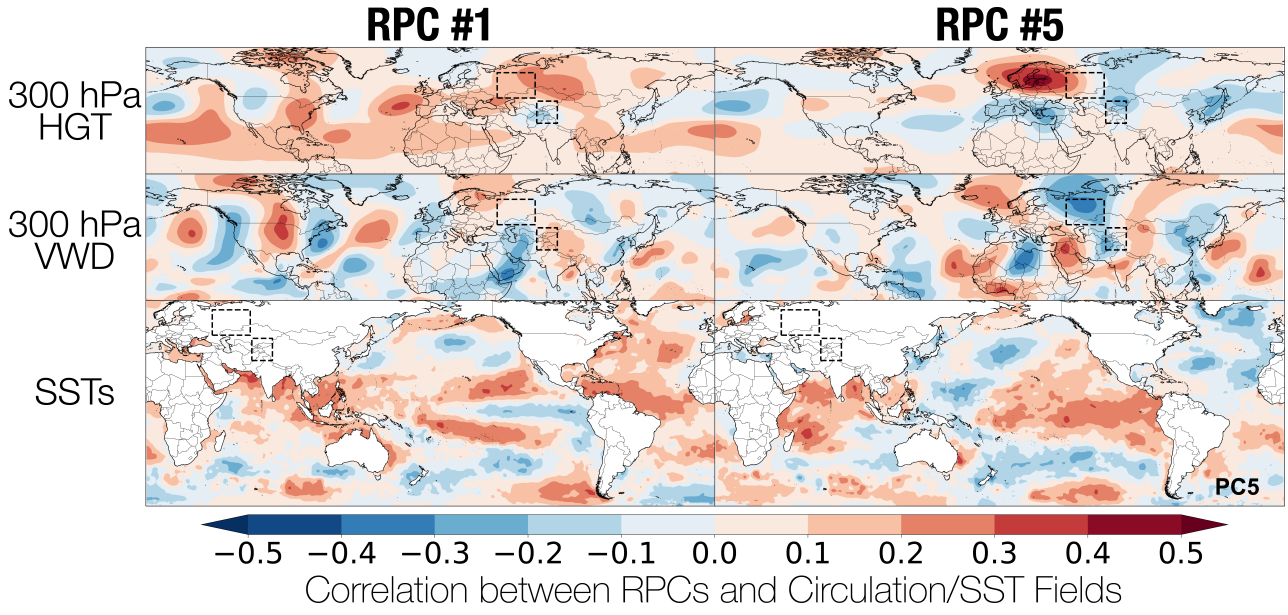

FIG. 7. Correlations (Pearson's r; 1901–2015) between RPC #1 and RPC #5 from the GEDA and JJA fields of 300 hPa geopotential heights, 300 hPa meriodional winds, and sea surface temperatures.

moisture, show patterns consistent with cyclonic circulation anomalies over Central Asia that would drive moisture into this region. Additionally, the 300 hPa meridional winds correlations across the Northern Hemisphere midlatitudes show a pattern similar to the wave train apparent in the $+1\sigma$ NPK composite anomalies in Figure 5. RCP #5 is strongly positively correlated with geopotential heights over northern Europe and western Russia and also cyclonic circulation over Central Asia, consistent with the strong relationship between this mode and drought over WRU. Both modes are positively correlated with SSTs in the northern Arabian Sea and Bay of Bengal, while the correlations with western tropical Indian Ocean SSTs are opposite between RPC #1 and #5. The two modes also have opposite sign correlation in the tropical Pacific.

d. Dynamics of Concurrent wet NPK–dry WRU Extremes

The 2010 concurrent extreme was associated with several major anomalies in atmospheric circulation and tropical SSTs (Figure 8) (Di Capua et al. 2021; Lau and Kim 2012). The 300 hPa geopotential height anomalies show an intense high pressure center over eastern Europe and western Russia, near the epicenter of the heat and drought in the WRU region (e.g., Figure 1). The 300 hPa meridional winds indicate that this high pressure was part of a pan-hemispheric Rossby wave

Accepted for publication in *Journal of Climate*. DOI 10.1175/JCLI-D-23-0773.1.

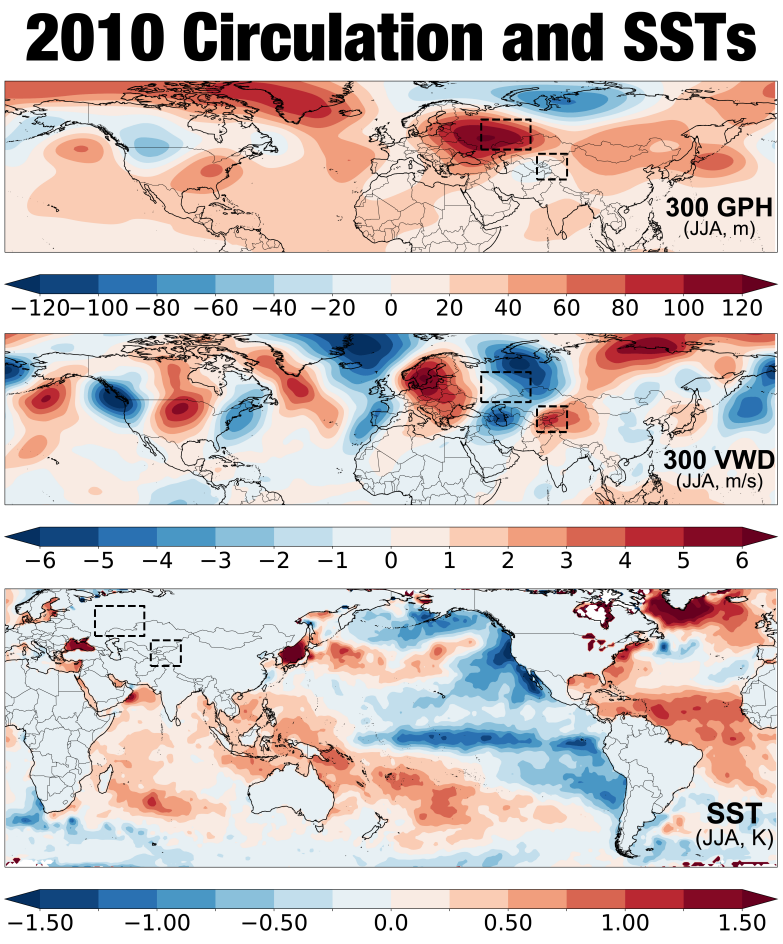

FIG. 8. Observed JJA circulation (300 hPa geopotential heights, m; meriodional winds; m/s) and sea surface temperature (K) anomalies during the 2010 wet NPK-dry WRU concurrent extreme event.

train, associated with anomalous northerly flow (negative anomalies) over WRU and southerly flow (positive anomalies) into NPK. Simultaneously, cold SSTs occurred across the tropical Pacific, part of the developing La Niña that would peak later in the year, along with anomalously warm SSTs in the Indian and tropical Atlantic basins.

Composite average circulation and SST anomalies for other instrumental era (1901–2015) concurrent wet NPK–dry WRU events show similar patterns to 2010 (Figure 9). For both definitions, these events are clearly associated with high pressure centered over western Russia, a hemispheric wave train reflected in the 300 hPa meridional winds, and cold SSTs in the tropical Pacific. The meridional wind anomalies over the North Atlantic are weaker in these composites compared to 2010, and the wave train itself appears to be better represented in the $+/-1\sigma$ definition. Tropical

Accepted for publication in *Journal of Climate*. DOI 10.1175/JCLI-D-23-0773.1.

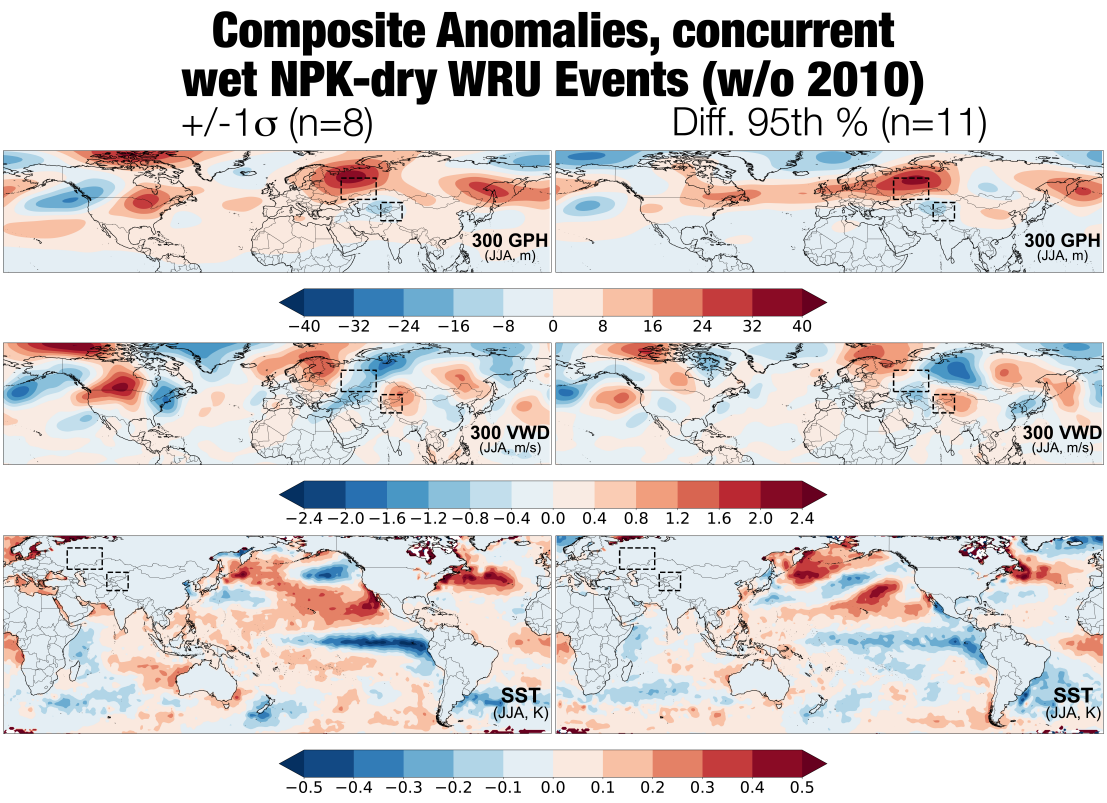

FIG. 9. Composite average JJA circulation (300 hPa geopotential heights, m; meriodional winds; m/s) and sea surface temperature anomalies (K) for all wet NPK-dry WRU concurrent extremes (1901–2015), excluding 2010. Years for the $+/-1\sigma$ events are: 1901, 1921, 1930, 1931, 1943, 1954, 1959, and 1988. For the 95th percentile difference events we use: 1901, 1921, 1930, 1931, 1951, 1959, 1967, 1975, 1981, 1988, and 1996.

Atlantic SST anomalies are also not nearly as warm in the composite relative to 2010. Generally, the anomaly fields reflect a mix of the composite anomalies for the single region events described previously (Figure 5). However, the concurrent event SST composite shows a strong La Niña association with cold tropical Pacific SSTs that is absent in either the -1σ WRU or $+1\sigma$ NPK composites.

Concurrent wet NPK-dry WRU events are strongly associated with positive values of RPCs #1 and #5 (Figure 10). All the wet NPK–dry WRU events we identified have positive values of RPC #1 (i.e., wet conditions in NPK) using the $+/-1\sigma$ definition, and 49 of 52 events (94%) are similarly positive under the 95th percentile definition. For RPC #5, the overwhelming majority (26 of 31 or 84% for the $+/-1\sigma$ definition; 44 of 52 or 85% for the 95th percentile definition) have positive values for RPC #5 (i.e., dry conditions in WRU). This strong association is confirmed when comparing

Accepted for publication in *Journal of Climate*. DOI 10.1175/JCLI-D-23-0773.1.

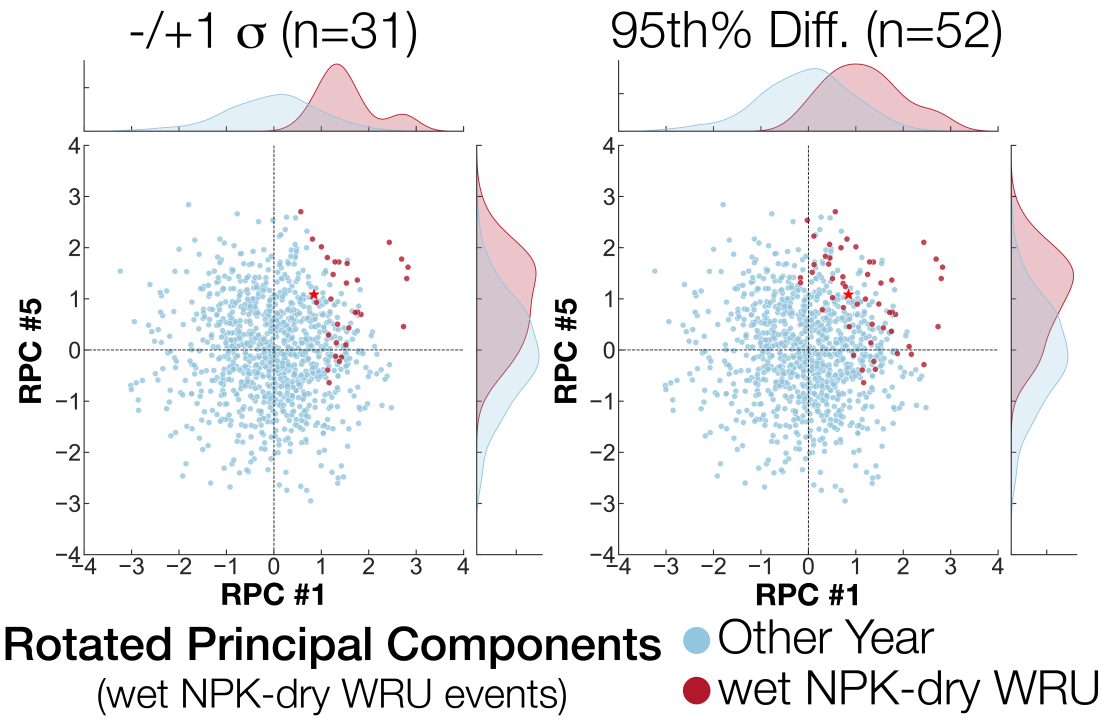

FIG. 10. Comparisons and distributions of PCs #1 and #5 for all years in the GEDA (blue dots and density plots) and for wet NPK-dry WRU events (red dots and density plots), based on our two definitions for these events. Red stars are the values for the 2010 event.

values for these PCs from the wet NPK–dry WRU events (Figure 10, red kernel density plots) against all other years in the reconstructions (Figure 10, blue kernel density plots), which show highly significant differences ($p \leq 0.01$; two-sided Wilcoxon Rank Sum and Kolmogorov-Smirnov tests). While neither RPC was extreme during the 2010 event, both modes were moderately positive: RPC #1= +0.84σ and RPC #5= +1.09σ (Figure 10, red stars).

4. Discussion and Conclusions

The 2010 concurrent extreme in western Russia and northern Pakistan is well captured in a seasonal reconstruction of JJA soil moisture, despite the sub-seasonal nature of both the heat wave in Russia and the extreme rainfall and flooding in Pakistan. We find that such events are quite rare over the last millennium, occurring in only 3–5% of years, and our study is the latest of several that demonstrate how seasonal tree-ring reconstructions can be used for analyses of sub-seasonal climate extremes (Borkotoky et al. 2021, 2023; Heeter et al. 2023; Steinschneider et al. 2018). These results suggest

Accepted for publication in *Journal of Climate*. DOI 10.1175/JCLI-D-23-0773.1.

that the 2010 event was characterized by (1) the second lowest soil moisture in WRU of the last 1,021 years and (2) the largest difference in soil moisture between NPK and WRU. Additionally, the reconstruction indicates that this event was made more likely by a post-1900 shift towards drier mean conditions in WRU and, though the evidence is weaker, wetter mean conditions in NPK. This change in risk is reflected in the much higher frequency of wet NPK–dry WRU concurrent extremes in the post-1900 period, during which 29% or 23% of events in the record have occurred, based on the $+/-1\sigma$ and 95$^{\text{th}}$ percentile difference definitions, respectively.

Despite its extreme magnitude, the soil moisture anomalies during the 2010 event were not associated with extreme values of the two RPCs in the GEDA that appear as the main drivers of wet NPK–dry WRU events over the last millennium. This may reflect the location of the strongest eigenvector weights, which are not precisely colocated with the regions of most intense soil moisture anomalies, and therefore may bring in additional information from less extreme regions. Alternatively, this could suggest the potential importance of contributions from other factors to 2010's intensity. One of the most comprehensive analyses of 2010 was conducted by Di Capua et al. (2021), who attributed this event to a combination of SST forcing from the tropics, dry soil moisture conditions in western Russia, and high-latitude warming that all combined to increase the occurrence and intensity of the Rossby wave train that was the proximal driver of this event. Much of Asia, including the area in which our NPK region is located, is also strongly influenced by anthropogenic aerosol forcing (Ratnam et al. 2021). While the conventional expectation is that aerosols will weaken monsoon precipitation by slowing the hydrologic cycle (Wang et al. 2022), there is evidence that aerosols can enhance mean and extreme precipitation, including over northwestern South Asia (Andreae et al. 2004; Guo et al. 2016; Lee et al. 2008; Singh et al. 2019, 2023). While the RPCs in the GEDA capture the local circulation anomalies and Rossby wave train pattern itself, the full suite of dynamics discussed by Di Capua et al. (2021) and others is unlikely to be fully resolved within these two modes.

There also remain outstanding questions regarding the extent to which climate change may have contributed to either the likelihood or intensity of the 2010 event. Simulations using modern radiative forcing find an increased risk of extreme heat in western Russia by a factor of 2 and heavy precipitation in northern Pakistan by a factor of 4 (Di Capua et al. 2021), but the process pathways for these contributions from anthropogenic forcing are uncertain. For example, while

Accepted for publication in *Journal of Climate*. DOI 10.1175/JCLI-D-23-0773.1.

climate change likely increased the heat wave risk over Russia directly through warmer overall temperatures (Di Capua et al. 2021; Hauser et al. 2016), it is less clear if increased radiative forcing contributed to the severe soil moisture deficits in this region, which amplified the local heat directly and the downstream Rossby wave response. The GEDA does show a drying soil moisture trend over WRU in the 20th century that would contribute towards the increased occurrence of wet NPK–dry WRU events in this interval. These trends are consistent with forced soil moisture responses in some model projections (Cook et al. 2020a), and at least tangentially support hypotheses regarding the role of climate change through this mechanism. An explicit climate change attribution analysis is, however, outside the scope of the current study.

While we believe our approach does offer value for studying events like 2010, we are cognizant of some of the inherent limitations in our use of seasonal reconstructions for analyses of higher temporal resolution events. The major soil moisture drying in western Russia occurred rapidly over a matter of weeks in early summer, with the most intense heat following in the mid-summer. In Pakistan, the flooding occurred as a consequence of several heavy rainfall events in July followed by an extended period of steady rainfall for almost the entirety of August (Lau and Kim 2012). These event evolutions cannot be resolved within a singular seasonal climate reconstruction. There are also potential uncertainties and biases in the tree-ring proxies themselves used for the reconstruction. For example, trees are typically much more sensitive to dry versus wet extremes, and therefore may underestimate the magnitude of extreme wet events (Fritts 1976; Wise and Dannenberg 2019). Trees also have strong seasonal biases in their climate response which may differ to some degree with the target reconstruction variable (St. George et al. 2010; St. George and Ault 2014). We are encouraged, however, by the strong validation statistics in the GEDA in WRU and NPK and our results demonstrating that events like 2010 can be resolved on a level that allows us to generate some insights regarding variability and mechanisms.

While quite rare, we identify numerous occurrences of wet NPK–dry WRU events in the GEDA over the last millennium that are similar to what occurred in 2010. This provides an important and much longer baseline relative to the instrumental record that can be used to contextualize and evaluate these extremes. In particular, spatial reconstructions like the GEDA may be especially useful for evaluating changes in the dynamics of extreme climate events, as evidenced by the correlations between RPCs #1 and #5 and the large-scale circulation fields. This is an important

Accepted for publication in *Journal of Climate*. DOI 10.1175/JCLI-D-23-0773.1.

avenue of research, as changes in the dynamics associated with extreme climate events are more difficult to detect and less well understood (Gagen et al. 2016) compared to much more well constrained thermodynamics shifts. With increasing evidence for their importance in recent extreme events (Di Capua and Rahmstorf 2023), there is potentially an important role for high resolution spatiotemporal paleoclimate reconstructions to contribute towards our understanding of the dynamics of these events now and in the past.

Accepted for publication in *Journal of Climate*. DOI 10.1175/JCLI-D-23-0773.1.

Acknowledgments. BIC supported by the NASA Modeling, Analysis, and Prediction program. KJA supported by the US National Science Foundation Paleoclimate Perspectives on Climate Change NSF AGS-1501856, AGS-1501834, and AGS-2102993.

Data availability statement. CRU TS monthly high-resolution gridded multivariate climate dataset: https://crudata.uea.ac.uk/cru/data/hrg/. CRU instrumental PDSI: https://crudata.uea.ac.uk/cru/data/drought/#global. Twentieth Century Reanalysis v3: https://psl.noaa.gov/data/20thC_Rean/. HadiSST Sea Surface Temperatures: https://www.metoffice.gov.uk/hadobs/hadisst/data/download.html. Great Eurasian Drought Atlas: https://www.dropbox.com/scl/fi/ejnoni5tt3zitxl5qqu48/geda_trim.nc?rlkey=g1edzlkgxkoqoppt9wll080q7&dl=0. NTREND WRU time series: https://www.dropbox.com/scl/fi/owapshyrtrdq244doomkw/russia_ntrend_extended_rescaled.txt?rlkey=lx0ynpp14aopy2q74azt776ga&dl=0.

References

Anchukaitis, K. J., and Coauthors, 2017: Last millennium Northern Hemisphere summer temperatures from tree rings: Part II, spatially resolved reconstructions. *Quaternary Science Reviews*, **163**, 1–22, https://doi.org/https://doi.org/10.1016/j.quascirev.2017.02.020, URL https://www.sciencedirect.com/science/article/pii/S0277379117301592.

Andreae, M. O., D. Rosenfeld, P. Artaxo, A. A. Costa, G. P. Frank, K. M. Longo, and M. A. F. Silva-Dias, 2004: Smoking Rain Clouds over the Amazon. *Science*, **303 (5662)**, 1337–1342, https://doi.org/10.1126/science.1092779, URL https://doi.org/10.1126/science.1092779.

Angélil, O., and Coauthors, 2016: Comparing regional precipitation and temperature extremes in climate model and reanalysis products. *Weather and Climate Extremes*, **13**, 35–43, https://doi.org/https://doi.org/10.1016/j.wace.2016.07.001, URL https://www.sciencedirect.com/science/article/pii/S2212094716300202.

Barichivich, J., T. Osborn, I. Harris, G. van der Schrier, and P. Jones, 2022: Monitoring global drought using the self-calibrating Palmer Drought Severity Index [in "State of the Climate in 2021"]. *Bulletin of the American Meteorological Society*, **103 (8)**, S31–S33, https://doi.org/https://doi.org/10.1175/BAMS-D-22-0092.1.

Accepted for publication in *Journal of Climate*. DOI 10.1175/JCLI-D-23-0773.1.

Barriopedro, D., E. M. Fischer, J. Luterbacher, R. M. Trigo, and R. García-Herrera, 2011: The Hot Summer of 2010: Redrawing the Temperature Record Map of Europe. *Science*, **332 (6026)**, 220–224, https://doi.org/10.1126/science.1201224, URL https://www.science.org/doi/abs/10.1126/science.1201224, https://www.science.org/doi/pdf/10.1126/science.1201224.

Borkotoky, S. S., A. P. Williams, E. R. Cook, and S. Steinschneider, 2021: Reconstructing Extreme Precipitation in the Sacramento River Watershed Using Tree-Ring Based Proxies of Cold-Season Precipitation. *Water Resources Research*, **57 (4)**, e2020WR028 824, https://doi.org/https://doi.org/10.1029/2020WR028824, URL https://doi.org/10.1029/2020WR028824.

Borkotoky, S. S., A. P. Williams, and S. Steinschneider, 2023: Six Hundred Years of Reconstructed Atmospheric River Activity Along the US West Coast. *Journal of Geophysical Research: Atmospheres*, **128 (12)**, e2022JD038 321, https://doi.org/https://doi.org/10.1029/2022JD038321, URL https://doi.org/10.1029/2022JD038321.

Bortnik, J., and E. Camporeale, 2021: Ten ways to apply machine learning in the Earth and space sciences. *Eos*, **102**, https://doi.org/https://doi.org/10.1029/2021EO160257.

Christian, J. I., J. B. Basara, E. D. Hunt, J. A. Otkin, and X. Xiao, 2020: Flash drought development and cascading impacts associated with the 2010 Russian heatwave. *Environmental Research Letters*, **15 (9)**, 094 078, https://doi.org/10.1088/1748-9326/ab9faf, URL https://dx.doi.org/10.1088/1748-9326/ab9faf.

Cook, B. I., J. S. Mankin, K. Marvel, A. P. Williams, J. E. Smerdon, and K. J. Anchukaitis, 2020a: Twenty-first Century Drought Projections in the CMIP6 Forcing Scenarios. *Earth's Future*, **n/a (n/a)**, e2019EF001 461, https://doi.org/10.1029/2019EF001461, URL https://doi.org/10.1029/2019EF001461.

Cook, E. R., K. J. Anchukaitis, B. M. Buckley, R. D. D'Arrigo, G. C. Jacoby, and W. E. Wright, 2010: Asian Monsoon Failure and Megadrought During the Last Millennium. *Science*, **328 (5977)**, 486–489, https://doi.org/10.1126/science.1185188, http://science.sciencemag.org/content/328/5977/486.full.pdf.

Cook, E. R., and Coauthors, 2015: Old World megadroughts and pluvials during the Common Era. *Science Advances*, **1 (10)**, https://doi.org/10.1126/sciadv.1500561.

Accepted for publication in *Journal of Climate*. DOI 10.1175/JCLI-D-23-0773.1.

Cook, E. R., and Coauthors, 2020b: The European Russia Drought Atlas (1400–2016 CE). *Climate Dynamics*, **54 (3)**, 2317–2335, https://doi.org/10.1007/s00382-019-05115-2, URL https://doi.org/10.1007/s00382-019-05115-2.

Cowtan, K., and R. G. Way, 2014: Coverage bias in the HadCRUT4 temperature series and its impact on recent temperature trends. *Quarterly Journal of the Royal Meteorological Society*, **140 (683)**, 1935–1944, https://doi.org/https://doi.org/10.1002/qj.2297, URL https://doi.org/10.1002/qj.2297.

Di Capua, G., and S. Rahmstorf, 2023: Extreme weather in a changing climate. *Environmental Research Letters*, **18 (10)**, 102 001, https://doi.org/10.1088/1748-9326/acfb23, URL https://dx.doi.org/10.1088/1748-9326/acfb23.

Di Capua, G., S. Sparrow, K. Kornhuber, E. Rousi, S. Osprey, D. Wallom, B. van den Hurk, and D. Coumou, 2021: Drivers behind the summer 2010 wave train leading to Russian heatwave and Pakistan flooding. *npj Climate and Atmospheric Science*, **4 (1)**, 55, https://doi.org/10.1038/s41612-021-00211-9, URL https://doi.org/10.1038/s41612-021-00211-9.

Dole, R., and Coauthors, 2011: Was there a basis for anticipating the 2010 Russian heat wave? *Geophysical Research Letters*, **38 (6)**, https://doi.org/https://doi.org/10.1029/2010GL046582, URL https://agupubs.onlinelibrary.wiley.com/doi/abs/10.1029/2010GL046582, https://agupubs.onlinelibrary.wiley.com/doi/pdf/10.1029/2010GL046582.

Esper, J., and Coauthors, 2018: Large-scale, millennial-length temperature reconstructions from tree-rings. *Dendrochronologia*, **50**, 81–90, https://doi.org/https://doi.org/10.1016/j.dendro.2018.06.001, URL https://www.sciencedirect.com/science/article/pii/S1125786518300687.

Fritts, H., 1976: *Tree Rings and Climate*. Elsevier.

Gagen, M. H., E. Zorita, D. McCarroll, M. Zahn, G. H. F. Young, and I. Robertson, 2016: North Atlantic summer storm tracks over Europe dominated by internal variability over the past millennium. *Nature Geoscience*, **9 (8)**, 630–635, https://doi.org/10.1038/ngeo2752, URL https://doi.org/10.1038/ngeo2752.

Guo, J., and Coauthors, 2016: Delaying precipitation and lightning by air pollution over the Pearl River Delta. Part I: Observational analyses. *Journal of Geophysical Research: Atmospheres*,

Accepted for publication in *Journal of Climate*. DOI 10.1175/JCLI-D-23-0773.1.

121 (11), 6472–6488, https://doi.org/https://doi.org/10.1002/2015JD023257, URL https://doi.org/10.1002/2015JD023257.

Harris, I., T. J. Osborn, P. Jones, and D. Lister, 2020: Version 4 of the CRU TS monthly high-resolution gridded multivariate climate dataset. *Scientific Data*, **7 (1)**, 109, https://doi.org/10.1038/s41597-020-0453-3, URL https://doi.org/10.1038/s41597-020-0453-3.

Hauser, M., R. Orth, and S. I. Seneviratne, 2016: Role of soil moisture versus recent climate change for the 2010 heat wave in western Russia. *Geophysical Research Letters*, **43 (6)**, 2819–2826, https://doi.org/10.1002/2016GL068036, URL https://doi.org/10.1002/2016GL068036.

Heeter, K. J., G. L. Harley, J. T. Abatzoglou, K. J. Anchukaitis, E. R. Cook, B. L. Coulthard, L. A. Dye, and I. K. Homfeld, 2023: Unprecedented 21st century heat across the Pacific Northwest of North America. *npj Climate and Atmospheric Science*, **6 (1)**, 5, https://doi.org/10.1038/s41612-023-00340-3, URL https://doi.org/10.1038/s41612-023-00340-3.

Houze, R. A., K. L. Rasmussen, S. Medina, S. R. Brodzik, and U. Romatschke, 2011: Anomalous Atmospheric Events Leading to the Summer 2010 Floods in Pakistan. *Bulletin of the American Meteorological Society*, **92 (3)**, 291 – 298, https://doi.org/https://doi.org/10.1175/2010BAMS3173.1, URL https://journals.ametsoc.org/view/journals/bams/92/3/2010bams3173_1.xml.

Hunt, E., and Coauthors, 2021: Agricultural and food security impacts from the 2010 Russia flash drought. *Weather and Climate Extremes*, **34**, 100 383, https://doi.org/https://doi.org/10.1016/j.wace.2021.100383, URL https://www.sciencedirect.com/science/article/pii/S2212094721000736.

Lau, W. K. M., and K.-M. Kim, 2012: The 2010 Pakistan Flood and Russian Heat Wave: Teleconnection of Hydrometeorological Extremes. *Journal of Hydrometeorology*, **13 (1)**, 392–403, https://doi.org/10.1175/JHM-D-11-016.1.

Lee, S. S., L. J. Donner, V. T. J. Phillips, and Y. Ming, 2008: Examination of aerosol effects on precipitation in deep convective clouds during the 1997 ARM summer experiment. *Quarterly Journal of the Royal Meteorological Society*, **134 (634)**, 1201–1220, https://doi.org/https://doi.org/10.1002/qj.287, URL https://doi.org/10.1002/qj.287.

Accepted for publication in *Journal of Climate*. DOI 10.1175/JCLI-D-23-0773.1.

Luo, F., and Coauthors, 2022: Summertime Rossby waves in climate models: substantial biases in surface imprint associated with small biases in upper-level circulation. *Weather and Climate Dynamics*, **3 (3)**, 905–935, https://doi.org/10.5194/wcd-3-905-2022, URL https://wcd.copernicus.org/articles/3/905/2022/.

Miralles, D. G., A. J. Teuling, C. C. van Heerwaarden, and J. Vila-Guerau de Arellano, 2014: Mega-heatwave temperatures due to combined soil desiccation and atmospheric heat accumulation. *Nature Geoscience*, **7 (5)**, 345–349, https://doi.org/doi:10.1038/ngeo2141.

Morice, C. P., J. J. Kennedy, N. A. Rayner, and P. D. Jones, 2012: Quantifying uncertainties in global and regional temperature change using an ensemble of observational estimates: The HadCRUT4 data set. *Journal of Geophysical Research: Atmospheres*, **117 (D8)**, https://doi.org/10.1029/2011JD017187, URL https://doi.org/10.1029/2011JD017187.

Palmer, W. C., 1965: Meteorological drought. Tech. rep., US Weather Bureau, Washington, DC, 1–58 pp.

Pederson, N., A. E. Hessl, N. Baatarbileg, K. J. Anchukaitis, and N. Di Cosmo, 2014: Pluvials, droughts, the Mongol Empire, and modern Mongolia. *Proceedings of the National Academy of Sciences*, **111 (12)**, 4375–4379, https://doi.org/10.1073/pnas.1318677111.

Priya, P., M. Mujumdar, T. P. Sabin, P. Terray, and R. Krishnan, 2015: Impacts of Indo-Pacific Sea Surface Temperature Anomalies on the Summer Monsoon Circulation and Heavy Precipitation over Northwest India–Pakistan Region during 2010. *Journal of Climate*, **28 (9)**, 3714–3730, https://doi.org/https://doi.org/10.1175/JCLI-D-14-00595.1, URL https://journals.ametsoc.org/view/journals/clim/28/9/jcli-d-14-00595.1.xml.

Ratnam, M. V., P. Prasad, S. T. A. Raj, M. R. Raman, and G. Basha, 2021: Changing patterns in aerosol vertical distribution over South and East Asia. *Scientific Reports*, **11 (1)**, 308, https://doi.org/10.1038/s41598-020-79361-4, URL https://doi.org/10.1038/s41598-020-79361-4.

Rayner, N. A., D. E. Parker, E. B. Horton, C. K. Folland, L. V. Alexander, D. P. Rowell, E. C. Kent, and A. Kaplan, 2003: Global analyses of sea surface temperature, sea ice, and night marine

Accepted for publication in *Journal of Climate*. DOI 10.1175/JCLI-D-23-0773.1.

air temperature since the late nineteenth century. *Journal of Geophysical Research*, **108 (D14)**, 4407, https://doi.org/10.1029/2002JD002670.

Robeson, S. M., J. T. Maxwell, and D. L. Ficklin, 2020: Bias Correction of Paleoclimatic Reconstructions: A New Look at 1,200+ Years of Upper Colorado River Flow. *Geophysical Research Letters*, **47 (1)**, e2019GL086 689, https://doi.org/https://doi.org/10.1029/2019GL086689, URL https://doi.org/10.1029/2019GL086689.

Schubert, S., H. Wang, and M. Suarez, 2011: Warm Season Subseasonal Variability and Climate Extremes in the Northern Hemisphere: The Role of Stationary Rossby Waves. *Journal of Climate*, **24 (18)**, 4773–4792, https://doi.org/10.1175/JCLI-D-10-05035.1.

Schubert, S. D., H. Wang, R. D. Koster, M. J. Suarez, and P. Y. Groisman, 2014: Northern Eurasian Heat Waves and Droughts. *Journal of Climate*, **27 (9)**, 3169–3207, https://doi.org/10.1175/JCLI-D-13-00360.1.

Shaposhnikov, D., and Coauthors, 2014: Mortality Related to Air Pollution with the Moscow Heat Wave and Wildfire of 2010. *Epidemiology*, **25 (3)**, URL https://journals.lww.com/epidem/fulltext/2014/05000/mortality_related_to_air_pollution_with_the_moscow.6.aspx.

Singh, D., M. Bollasina, M. Ting, and N. S. Diffenbaugh, 2019: Disentangling the influence of local and remote anthropogenic aerosols on South Asian monsoon daily rainfall characteristics. *Climate Dynamics*, **52 (9)**, 6301–6320, https://doi.org/10.1007/s00382-018-4512-9, URL https://doi.org/10.1007/s00382-018-4512-9.

Singh, J., B. I. Cook, K. Marvel, S. McDermid, G. G. Persad, B. Rajaratnam, and D. Singh, 2023: Anthropogenic Aerosols Delay the Emergence of GHGs-Forced Wetting of South Asian Rainy Seasons Under a Fossil-Fuel Intensive Pathway. *Geophysical Research Letters*, **50 (18)**, e2023GL103 949, https://doi.org/https://doi.org/10.1029/2023GL103949, URL https://doi.org/10.1029/2023GL103949.

Slivinski, L. C., and Coauthors, 2021: An Evaluation of the Performance of the Twentieth Century Reanalysis Version 3. *Journal of Climate*, **34 (4)**, 1417 – 1438, https://doi.org/https://doi.org/10.1175/JCLI-D-20-0505.1, URL https://journals.ametsoc.org/view/journals/clim/34/4/JCLI-D-20-0505.1.xml.

Accepted for publication in *Journal of Climate*. DOI 10.1175/JCLI-D-23-0773.1.

Smerdon, J. E., E. R. Cook, and N. J. Steiger, 2023: The Historical Development of Large-Scale Paleoclimate Field Reconstructions Over the Common Era. *Reviews of Geophysics*, **61 (4)**, e2022RG000 782, https://doi.org/https://doi.org/10.1029/2022RG000782, URL https://doi.org/10.1029/2022RG000782.

St. George, S., and T. R. Ault, 2014: The imprint of climate within Northern Hemisphere trees. *Quaternary Science Reviews*, **89**, 1–4, https://doi.org/https://doi.org/10.1016/j.quascirev.2014.01.007.

St. George, S., D. Meko, and E. Cook, 2010: The seasonality of precipitation signals embedded within the North American Drought Atlas. *The Holocene*, **20 (6)**, 983–988, https://doi.org/10.1177/0959683610365937.

Steinschneider, S., M. Ho, A. P. Williams, E. R. Cook, and U. Lall, 2018: A 500-Year Tree Ring-Based Reconstruction of Extreme Cold-Season Precipitation and Number of Atmospheric River Landfalls Across the Southwestern United States. *Geophysical Research Letters*, **45 (11)**, 5672–5680, https://doi.org/https://doi.org/10.1029/2018GL078089, URL https://doi.org/10.1029/2018GL078089.

van der Schrier, G., J. Barichivich, K. R. Briffa, and P. D. Jones, 2013: A scPDSI-based global data set of dry and wet spells for 1901–2009. *Journal of Geophysical Research: Atmospheres*, https://doi.org/10.1002/jgrd.50355.

Wang, Z., L. Xue, J. Liu, K. Ding, S. Lou, A. Ding, J. Wang, and X. Huang, 2022: Roles of Atmospheric Aerosols in Extreme Meteorological Events: a Systematic Review. *Current Pollution Reports*, **8 (2)**, 177–188, https://doi.org/10.1007/s40726-022-00216-9, URL https://doi.org/10.1007/s40726-022-00216-9.

Webster, P. J., V. E. Toma, and H. M. Kim, 2011: Were the 2010 Pakistan floods predictable? *Geophysical Research Letters*, **38 (4)**, https://doi.org/https://doi.org/10.1029/2010GL046346, URL https://doi.org/10.1029/2010GL046346.

Wells, N., S. Goddard, and M. J. Hayes, 2004: A Self-Calibrating Palmer Drought Severity Index. *Journal of Climate*, **17 (12)**, 2335–2351, https://doi.org/10.1175/1520-0442(2004)017⟨2335:ASPDSI⟩2.0.CO;2.

Accepted for publication in *Journal of Climate*. DOI 10.1175/JCLI-D-23-0773.1.

White, R. H., K. Kornhuber, O. Martius, and V. Wirth, 2022: From Atmospheric Waves to Heatwaves: A Waveguide Perspective for Understanding and Predicting Concurrent, Persistent, and Extreme Extratropical Weather. *Bulletin of the American Meteorological Society*, **103 (3)**, E923–E935, https://doi.org/https://doi.org/10.1175/BAMS-D-21-0170.1, URL https://journals.ametsoc.org/view/journals/bams/103/3/BAMS-D-21-0170.1.xml.

Wilson, R., and Coauthors, 2016: Last millennium northern hemisphere summer temperatures from tree rings: Part I: The long term context. *Quaternary Science Reviews*, **134**, 1–18, https://doi.org/https://doi.org/10.1016/j.quascirev.2015.12.005, URL https://www.sciencedirect.com/science/article/pii/S0277379115301888.

Wise, E. K., and M. P. Dannenberg, 2019: Climate Factors Leading to Asymmetric Extreme Capture in the Tree-Ring Record. *Geophysical Research Letters*, **46 (6)**, 3408–3416, https://doi.org/https://doi.org/10.1029/2019GL082295, URL https://doi.org/10.1029/2019GL082295.

Wright, C. S., 1975: Soviet Farm Failures. *New York Times*.

Accepted for publication in *Journal of Climate*. DOI 10.1175/JCLI-D-23-0773.1.